Optical near-field absorption at a metal tip far from plasmonic resonance

J. Houard,* A. Vella, F. Vurpillot, and B. Deconihout
Groupe de Physique des Materiaux, UMR CNRS 6634, UFR Sciences Site du Madrillet, Avenue de l'Université-BP 12, 76801 Saint Etienne Du Rouvray Cedex, France
(Received 3 February 2010; published 12 March 2010)

We investigate the wavelength and the polarization dependence of the absorption of a subwavelength tip illuminated by an ultrashort laser pulse using laser-assisted atom-probe tomography. We show that it is possible to localize the absorption at the tip apex by choosing the appropriate laser polarization and wavelength even for excitation wavelength far from the plasmonic resonance. This effect can be explained by the diffraction theory of Sommerfeld applied on a tip geometry. Furthermore, numerical calculations are performed on a real subwavelength tip to confirm this absorption localization and to explain the role of the polarization and the wavelength.

DOI: 10.1103/PhysRevB.81.125411 PACS number(s): 68.37.Vj, 68.37.Uv, 78.67.−n, 79.70.+q

Many techniques of materials analysis or materials structuring are based on the interaction of a light source with the apex of a sharply pointed metallic needle with subwavelength dimensions (named as a tip). The enhancement phenomenon occurring at the apex of the tip increases the intrinsic electromagnetic field by several hundreds, especially in the case of metals such as silver or gold.[1] This field can be used to make nanotweezer or to generate a localized excitation on the surface of a planar substrate, in photoassisted scanning tunneling microscopy and in apertureless near-field optical microscopy, for instance.[1–3] At higher light intensity, this extreme localization can be used as a sharp tool to modify the surface of the substrate.[4] In all these techniques, it is important to maximize the optical field at the apex of the tip, without significantly increasing the temperature of the tip itself. Indeed, if the light absorption at the end of the needle is too high, tip expansion or even tip melting can occur.[2,5] It is worth noting that this undesirable expansion is usually calculated or simulated assuming a heated zone equal to the laser waist. Only in the case of resonant excitation of surface plasmon, it was shown that the size of the heated zone becomes very small (<100 nm) and the maximum of the temperature is reached inside the tip at about 20 nm away from the surface.[1] Clearly, it is important to verify if in the "nonresonant" conditions, the absorption at the tip apex takes place on a region much smaller than the waist, otherwise common models might have to be reconsidered. In addition, in the case of resonant excitation, the physical origin of the absorption localization is well known (strong lighting rod effect), however for nonresonant excitation, it is important to determine the physical parameters allowing the control of the absorption extent.

Such a study might also be of interest in techniques where the energy has to be localized at the very end apex of the tip. For instance, a very confined absorption is required in photoassisted field-electron (FE) emission or in laser-assisted atom-probe tomography (APT). In FE, using femtosecond (fs) laser pulses, it was shown that ultrashort electron pulses can be generated.[6,7] To increase the temporal resolution and the brightness of these electron sources, an emission region as small as possible (in the nanometer range) is necessary. Therefore, it is important to maximize and to confine the photoabsorption at the tip apex. In the APT, surface atoms are emitted from a tip in form of ions by the combined action of a standing electrostatic field and a laser pulse that triggers the ion emission. Recent results have shown that the absorption of the laser energy by the tip increases the tip surface temperature leading to the evaporation of atoms.[8,9] Since this emission results from the thermal response of the tip to the fs light pulse, both the heating and cooling times must be optimized to increase the APT timing resolution. The key factors governing the cooling time are the thermal diffusivity (D) of the material and the size of the heated zone w, $\tau_{cooling} \approx w^2/D$. In order to minimize this time $\tau_{cooling}$, the heating must be strongly confined at the tip apex. One might think to achieve this confinement by decreasing the laser spot size. However this only brings a very small change even when a strong focusing is used as shown by Bunton *et al.*[10]

In this study, based on theoretical considerations, it is shown that the extent of the area where the absorption takes place can be chosen by adjusting the wavelength and the direction of the laser polarization. This allows to get a strong confinement of the absorption or, conversely, to avoid this confinement when necessary. In addition, APT is used as a very sensitive temperature probe to experimentally verify these conditions. Numerical resolution of Maxwell equations on an actual tip geometry are eventually performed to interpret the role of the wavelength and of the linear polarization direction.

The paper is organized as follows: in the first section, after a short reminder of the laser-assisted field evaporation process, our experimental results are presented. In the second section, experimental results are discussed proposing a model supported by numerical calculations on the real tip geometry. Eventually, in the last section, our conclusions are drawn.

I. MEASUREMENT OF ABSORPTION AREA BY APT

A. Experimental setup

The instrument used in this study is a linear three-dimensional (3D) atom probe assisted by femtosecond laser pulses and equipped with a multihit position sensitive detector (timing accuracy of 1 ns full width at half maximum).[11]

Experiments are done in ultrahigh vacuum ($<10^{-7}$ Pa), and the specimen is cooled down at cryogenic temperature (T_0 =80 K). The laser system is an amplified Ti:sapphire laser (wavelength λ=780 nm, frequency 1 kHz, pulse duration 130 fs, and pulse energy up to 2.5 mJ/pulse). The system is combined with an optical parametric amplifier (TOPAS from Light Conversion) allowing to continuously tune wavelength between 280 and 2600 nm.[12] The linear polarized laser beam is focused on the tip apex with a spot of 0.8 mm. Ions are emitted by the combined action of a standing field and the laser pulse. The standing field is set at about 80% of the evaporation field, i.e., the field necessary to achieve evaporation when no laser pulse is applied.[13,14]

B. Evaporation rate for axial linear polarization

Considering the field evaporation theory of a field emitter, surface atoms are emitted with an evaporation rate $K(t)$ given by

$$K(t) = N \times \nu \times \exp\left[\frac{-Q_n}{k_B T(t)}\right] \quad (1)$$

with N the number of kink site surface atoms, ν the surface-atom vibration frequency, k_B the Boltzmann's constant ($\approx 8.6\times 10^{-5}$ eV K^{-1}), and Q_n the activation energy ($\approx$0.1–1 eV). As a result, the temperature variation in the tip apex can be scanned as a function of time by measuring $K(t)$.

This field evaporation rate is measured as a function of time in axial linear polarization condition (laser field parallel to the tip axis). Only the laser wavelength λ is changed, all other parameters being kept constant.

The relationship between the initial distribution of the temperature in the tip and the decay of the temperature at the apex was theoretically calculated in the case of a semi-infinite cylinder assuming a constant diffusivity D [hot wire model (HWM)].[8] In this model, the initial temperature distribution has a Gaussian shape centered at the tip apex with a width equal to the heated zone w, and an amplitude $T_{\max}$, the maximal temperature reached after the laser illumination. The cooling rate is governed by

$$T(t) \approx \frac{T_{\max}}{\sqrt{1+\frac{2D}{w^2}\times t}}. \quad (2)$$

Due to the exponential decay of the evaporation rate $K(t)$, most of the atoms are evaporated in the very first moments of the cooling process. Then, we define the evaporation time τ_{evap} as the time at which $K(t)$ is divided by 10. Inserting Eq. (2) in Eq. (1), and taking $(k_B T_{\max})/Q_n$=5% from Ref. 8, τ_{evap} is given by

$$\tau_{evap} = \ln(10) \times \frac{k_B T_{\max}}{Q_n} \times \frac{w^2}{D} \approx 0.1\frac{w^2}{D}. \quad (3)$$

Hence, measuring the evaporation time using APT, an estimate of the size of the heated zone can be obtained and a study of the absorption confinement can be made.

The evaporation rate as a function of time, as measured from an aluminum tip and a stainless-steel tip are shown in Fig. 1. The shape of the aluminum tip and the stainless-steel tip, are approximately the same with a tip-end radius R =55±5 nm and a cone angle below 10°, as measured by transmission electron microscopy. The wavelength was tuned between 320 and 1600 nm and the polarization was set axial. The evaporation-rate measurement is derived from ion flight time spectra. Each spectrum is sampled over more than 50 000 evaporated atoms.

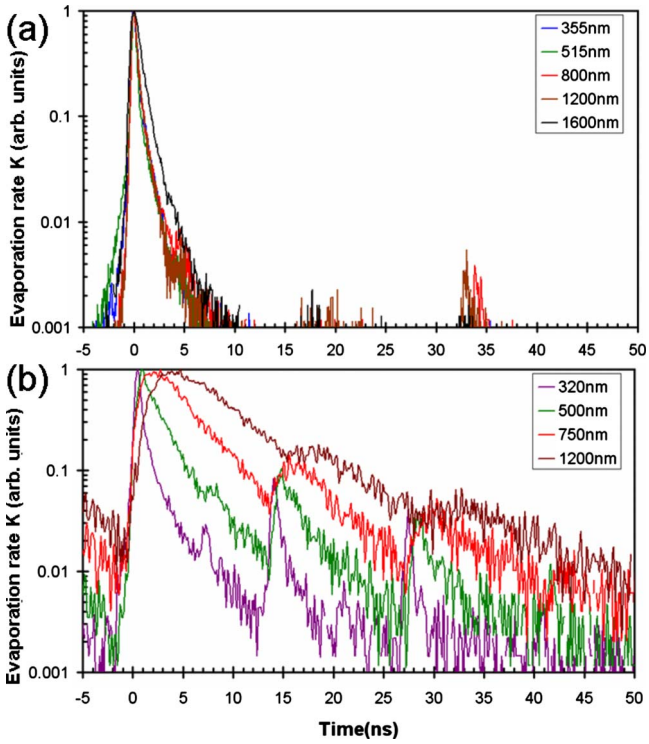

FIG. 1. (Color online) Evaporation rate as a function of time obtained (a) from an aluminum tip and (b) from a stainless-steel tip, for different wavelengths in axial polarization.

τ_{evap} for aluminum is extremely short [Fig. 1(a)]. For λ =1600 nm, τ_{evap} is 2.5 ns while for all other wavelengths it is 1.5 ns. This time corresponds to the detector timing resolution. Considering Eq. (3), and taking in account the thermal diffusivity of aluminum ($D_{\mathrm{Al}} \approx 10^{-4}$ m^2 s^{-1}), the size of the heated zone for λ=1200 nm is $w \approx 1200$ and $\approx$1600 nm for λ=1600 nm. Thus, in axial polarization and for infrared radiation, the size of the heated zone is roughly equal to the wavelength. However for shorter wavelengths, no conclusion can be drawn because of the too fast cooling time as compared to the detector timing accuracy. Same experiments were then performed on a stainless-steel tip ($Fe_{0.7}Cr_{0.19}Ni_{0.07}Si_{0.03}$), the thermal diffusivity of which is 20 times smaller than aluminum ($D_{steel} \approx 5\times 10^{-6}$ m^2 s^{-1}). In this case, the dependence of τ_{evap} on λ is clearly evidenced, as shown in Fig. 1(b). It increases with the laser wavelength from $\tau_{evap} \approx 2$ ns for λ=320 nm up to 20 ns for λ =1200 nm, corresponding to a heated size ranging from w $\approx$300 nm to $w \approx 1$ μm. Hence, also for a visible radiation, the tip is heated by the laser pulse on an area smaller than the wavelength. Note the presence in the spectra of delayed peaks due to ions with higher mass than ^{56}Fe. More unexpectedly, the peaks present a slow rising edge at longer

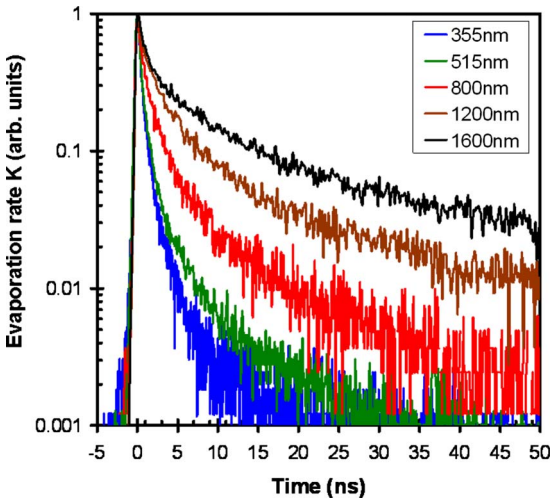

FIG. 2. (Color online) Evaporation rate as a function of time obtained from an aluminum tip at different wavelengths in transverse polarization.

wavelengths. Following the HWM model, the heated zone corresponds to the width of a Gaussian temperature distribution centered on the tip apex. If, due to the absorption process, the maximum temperature is not located on the tip end but somewhere further on the shank, the maximum evaporation rate is not reached just after the laser pulse but a time τ_{rise} later, due to the thermal diffusivity. From Fig. 1(b), τ_{rise} is evaluated to 5 ns for $\lambda=1200$ nm and to 2.8 ns for $\lambda=750$ nm. The position Z_0 of this maximum temperature can be evaluated using the diffusivity time law, $Z_0=\sqrt{D_{steel}\tau_{rise}}$. For $\lambda=1200$ nm, $Z_0\approx 220$ nm and for $\lambda=750$ nm, $Z_0\approx 170$ nm, i.e., a small fraction of the value of the wavelength.

C. Evaporation rate for transverse polarization

The field evaporation rate is measured as a function of time in transverse condition (laser field perpendicular to the tip axis), on the same Al tip. Only the laser wavelength λ is changed, all other parameters being kept constant. Figure 2 shows that the evaporation time strongly depends on λ.

τ_{evap} increases with the laser wavelength from $\tau_{evap}\approx 2$ ns for $\lambda=360$ nm up to 16 ns for $\lambda=1600$ nm, corresponding to a heated size ranging from $w\approx 1.4$ μm to $w\approx 4$ μm. Hence, also for a visible radiation, the tip is heated by the laser pulse on an area larger than the wavelength.

II. ANALYTICAL AND NUMERICAL MODELS

In order to explain why the heated area depends on λ and why the position of the temperature peak is not always located on the tip apex, diffraction effects on a medium with a tiplike shape features has to be considered. Rigorous calculations of near-field diffraction were done by Sommerfeld[15,16] on a half infinite plate, perfectly conductive, infinitely thin, and enlightened perpendicularly to the half plate with p-polarized light. An expression in terms of Fresnel integrals of the current density J was obtained,

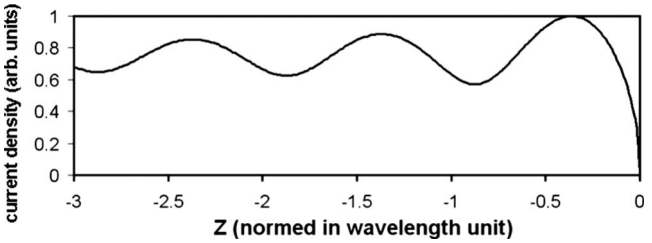

FIG. 3. Computed current density along a half infinite conducted plane. Note z axis corresponds to the distance from the free space.

$$J_Z=-\frac{c}{\pi\sqrt{\pi}}e^{i\pi/4}e^{ikZ}\mathcal{G}\{\sqrt{kZ}\}, \tag{4}$$

where $\vec{k}$ is the wave vector of the incident beam and $\mathcal{G}$ is a function of Fresnel integral,

$$\mathcal{G}(a)=e^{-ia^2}\int_a^{+\infty}e^{i\mu^2}d\mu. \tag{5}$$

For $kZ\gg 1$, a simple expression of J is obtained

$$J_Z=-\frac{c}{\pi\sqrt{\pi}}e^{i\pi/4}e^{ikZ}\frac{i}{2\sqrt{kZ}} \tag{6}$$

showing an oscillating behaviors of the current density with a periodicity equal to the laser wavelength. Note that the amplitude of the oscillation decreases as a function of $Z:(\frac{1}{\sqrt{kZ}})$, hence the maximum current density is localized near the edge of the plate. On real metallic materials, the absorption properties are linked to the surface current density through their conductivities. The shape of the real part of the current density of Eq. (4) is presented in Fig. 3 for p-polarized incident light.

Here $Z<0$ is the position on the plate, free space corresponds to $Z>0$, and $Z=0$ is the position of the edge of the plate. The oscillating behavior of J with a period equal to λ is confirmed.

In the case of a tip, the apex acts as a diffraction source emitting in all directions. This source interacts with the incident and the reflected beam giving rise to oscillating surface currents on the shank surface. It leads in the case of nonperfectly conductive material to absorption maxima.

To take into account the actual tip geometry and its optical properties, absorption 3D maps are computed by finite-difference time domain (FDTD) with a commercial software from Lumerical. In this model, the tip is represented as a cone terminated by a hemispheric cap. It is placed in the simulated space and surrounded by perfectly match layer avoiding any field reflection. For all wavelengths, the material properties are taken into account by using the dielectric constant taken from Ref. 17. The computation of the divergence of the Poynting vector leads to the 3D maps presented in Fig. 4 at $\lambda=355$ nm and $\lambda=1200$ nm on aluminum. First, an oscillation of the absorption with a period equal to λ is observed, as predicted by the former Sommerfeld model.

In order to evaluate the temperature rise along the tip axis, absorption density profiles along Z axis are presented in Fig.

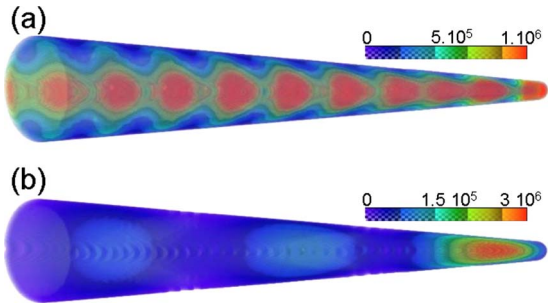

FIG. 4. (Color online) Absorption maps calculated by FDTD on the illuminated side of the Al tip for axial polarization, at (a) $\lambda = 355$ nm and at (b) $\lambda = 1200$ nm. The color bar is in (W m^{-3}) and corresponds to the power absorption density for an incoming intensity of 1 W m^{-2}.

5. Only the end of the tip is heated and a few micrometers away from the apex, the energy absorbed rapidly decays to zero. It means that the tip-apex temperature decays rapidly, explaining why in Fig. 1(a) no ion emission is observed a few nanoseconds after the maximum peak emission. In addition, the first absorption maximum is located at $\lambda/4$ from the tip apex as shown in Fig. 5 for the larger wavelengths. This is consistent with the slow rise time observed in Fig. 1(b). For shorter wavelengths $\lambda = 515$ nm or $\lambda = 360$ nm, the laser excitation is close to the tip surface-plasmon resonance and, as calculated by Novotny *et al.*,[1] the first absorption maximum is localized very close to the apex of the tip (as shown in the inset of Fig. 5 for $\lambda = 355$ nm and $\lambda = 515$ nm; the first peak is located at $Z = 20$ nm). It can be noticed that the shape of absorption maps is the same for steel and aluminum. Only the absolute amplitude of the absorption changes.

The absorption maps computed for transverse polarization excitation at $\lambda = 360$ nm [Fig. 6(a)] and at $\lambda = 1200$ nm [Fig. 6(b)], show that, in this configuration, the absorption of the shank becomes important and that no absorption oscillation is observed along the tip, conversely to the axial configuration. For $\lambda = 360$ nm, a red arrow shows the resonant absorption at the end of the tip [Fig. 6(a)]. In fact, this effect occurs when the ratio $R/\lambda \approx 0.15$ as showed by authors in Ref. 9. The absorption density profile, shown in Fig. 6(c), has two contributions. A sharp one localized on the "nanoparticle" which terminates the tip and a large one induced by the absorption of the shank (width >1 μm). The shank contribution increases with the wavelength whereas the amplitude of the sharp one decreases. As a result, for the larger wavelengths, the evaporation rate and then the apex temperature remains significant at long delay >10 ns after the laser pulse and for shorter wavelength, the evaporation rate decays rapidly (Fig. 2). Nevertheless, conversely to the axial case, 10 ns after the laser pulse, there is still ions emission due to the high absorption on the shank. Therefore, the wavelength evaporation-rate dependence in transverse mode is well explained by these absorption computations.

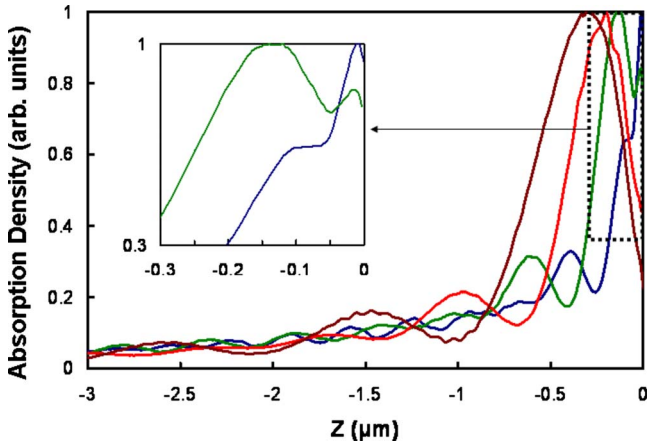

FIG. 5. (Color online) Normalized absorption density profile along the tip axis computed with previous maps for $\lambda = 360$ nm (blue), $\lambda = 515$ nm (green), $\lambda = 800$ nm (red), and $\lambda = 1200$ nm (brown). Inset: zoom of absorption profiles at the end of the tip for $\lambda = 360$ nm (blue) and for $\lambda = 515$ nm (green).

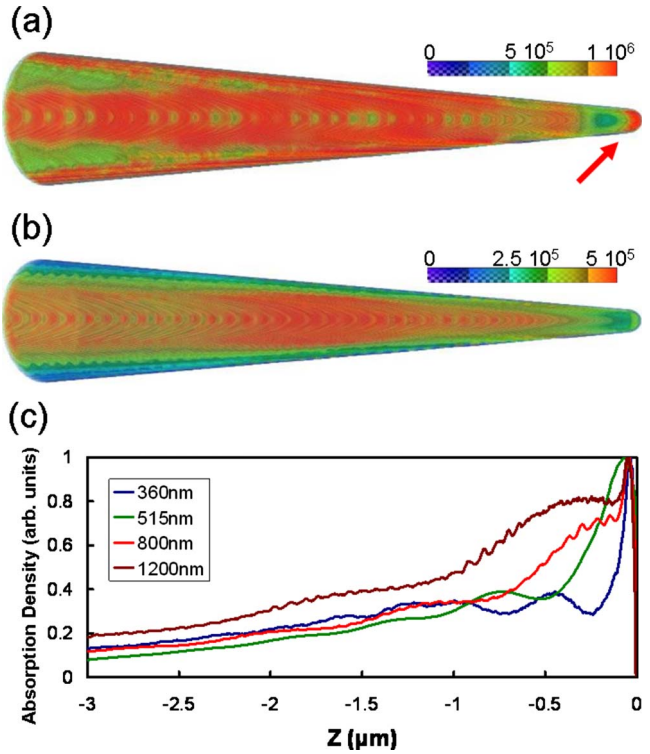

FIG. 6. (Color online) Absorption maps on Al tip in transverse polarization at (a) $\lambda = 355$ nm and at (b) $\lambda = 1200$ nm. Note on (a) the red arrow showing the resonant absorption of the *nanoparticle* which terminate the tip. (c) Normalized absorption density profile along the tip computed from the previous maps.

III. CONCLUSION

As a conclusion, it is possible to confine the absorption at the apex of a tip also for excitation far from the plasmonic one, thanks to the geometrical effects. Moreover, the size of the absorption zone can be adjusted by changing laser polarization and wavelength. These results are important for several reasons. First, they end the debate around the physical process involved in the laser-assisted field evaporation in APT. This process is clearly thermal and the confinement of

the absorption, predicted by this study, explains well the experimental observations. These results are also of great importance in other fields such as FE or near-field microscopy. The brightness and the size of the ultrashort electron pulses are clearly related to the absorption features of the field emitter. Furthermore, for near-field microscopy, the absorption confinement can explain the discrepancies experimentally observed changing the laser wavelength or the tip shape.[18] The presented absorption maps might be inserted in the expansion models. However, our study was done for a tip without any substrate in its near field, hence some refinements are necessary.

*jonathan.houard@etu.univ-rouen.fr

[1] L. Novotny, R. X. Bian, and X. S. Xie, Phys. Rev. Lett. **79**, 645 (1997).
[2] S. Grafström, P. Schuller, and J. Kowalski, J. Appl. Phys. **83**, 3453 (1998).
[3] R. Ossikovski, Q. Nguyen, and G. Picardi, Phys. Rev. B **75**, 045412 (2007).
[4] A. Kirsanov, A. Kiselev, A. Stepanov, and N. Polushkin, J. Appl. Phys. **94**, 6822 (2003).
[5] V. Gerstner, A. Knoll, W. Pfeiffer, A. Thon, and G. Gerber, J. Appl. Phys. **88**, 4851 (2000).
[6] P. Hommelhoff, Y. Sortais, A. Aghajani-Talesh, and M. A. Kasevich, Phys. Rev. Lett. **96**, 077401 (2006).
[7] C. Ropers, D. R. Solli, C. P. Schulz, C. Lienau, and T. Elsaesser, Phys. Rev. Lett. **98**, 043907 (2007).
[8] F. Vurpillot, J. Houard, A. Vella, and B. Deconihout, J. Phys. D **42**, 125502 (2009).
[9] J. Houard, A. Vella, F. Vurpillot, and B. Deconihout, Appl. Phys. Lett. **94**, 121905 (2009).
[10] J. H. Bunton, J. D. Olson, D. R. Lenz, and T. F. Kelly, Microsc. Microanal. **13**, 418 (2007).
[11] G. Da Costa, F. Vurpillot, A. Bostel, M. Bouet, and B. Deconihout, Rev. Sci. Instrum. **76**, 013304 (2005).
[12] B. Gault, F. Vurpillot, A. Vella, A. Bostel, A. Menand, and B. Deconihout, Rev. Sci. Instrum. **77**, 043705 (2006).
[13] E. W. Müller, Naturwiss. **29**, 533 (1941).
[14] R. Gomer, J. Chem. Phys. **31**, 341 (1959).
[15] A. Sommerfeld, Math. Ann. **47**, 317 (1896).
[16] M. Born and E. Wolf, *Principles of Optics*, 7th ed. (Cambridge University Press, Cambridge, England, 1999), pp. 633–657.
[17] E. Palik and G. Ghosh, *Handbook of Optical Constants of Solids* (Academic, New York, 1985).
[18] A. Chimmalgi, C. P. Grigoropoulos, and K. Komvopoulos, J. Appl. Phys. **97**, 104319 (2005).